RECENT ADVANCES IN PREDICTING THE DEVELOPMENT OF STRUCTURE IN MESOPHASE PITCH

A. D. Rey[1] and D. D. Edie[2]
[1] *McGill University, Montreal, Canada*
[2] *Clemson University, Clemson, SC, USA*

Corresponding author e-mail address: alejandro.rey@mcgill.ca

Introduction

This paper summarizes recent advances in our understanding of the relationship between mesophase structure and flow. Our research groups at Clemson and McGill have collaborated over the past six years in this investigation. Initially, the Clemson group developed the experimental procedures for accurately measuring the elastic and viscous effects of mesophase in both steady and transient flows. They then applied these procedures to measure the flow behavior of a well-characterized mesophase pitch. The McGill group developed a constitutive equation for this liquid material. The Clemson data were then used to test the McGill model. The results show that the model accurately predicts the formation and stability of mesophase structure during processing and explains the experimental observations made by White, Fathollahi, Edie, Fleurot and others [1-5].

Experimental

Materials: The mesophase used in this study was produced by Mitsubishi Gas Chemical Company (MGCC) and had a designation of ARA24R Lot# 6U21. The Mettler softening point, which is the ASTM standard for pitch softening point determination, was found to be 296.2°C.

Steady Rheological Measurements at Low Shear Rates: An ARES rheometer, built by Rheometric Scientific, was used to measure the low shear rate flow behavior of the mesophase. This instrument was equipped with 50 mm cone and plate fixtures, a Force Rebalance Transducer and an air-bearing LS motor. This configuration allows the ARES to accurately measure torque values as low as 0.02 g·cm and determine normal stresses with a high degree of precision.

Prior to testing the rheological behavior of mesophase pitch, cylindrical samples were created using a vacuum pelletization technique. The exact procedure for preparing the pellets is detailed by Cato [6]. At the start of each steady-state test the sample chamber of the instrument was purged with nitrogen to prevent oxidation of the pitch sample and the sample heated to the desired temperature. After thermal equilibrium was reached, a

pre-shear step was applied to the sample, and then the sample was allowed to rest for twenty to thirty minutes. Once this was accomplished, the steady-shear test was initiated. The precise step-by-step procedure used to obtain steady shear data is given in Cato [6].

Transient Rheological Measurements: An RDS-II rheometer, also built by Rheometrics Scientific, with 25 mm cone and plate fixtures was used to measure the transient shear properties of mesophase pitch. Once the rheometer was heated to the desired temperature, a pelletized sample was placed between the cone and plate and held until thermal equilibrium was reached. The sample was pre-sheared before measuring the transient shear behavior of the sample.

After the sample was pre-sheared, the sample was subjected to a four-step sequence of alternating periods of shear and rest (Figure 1 illustrates a typical four-step sequence). The instrument recorded the shear rate during each period along with the variation of shear stress on the cone with time. These transient data provided valuable information on both stress overshoot (as rotation was initiated during periods one and three) and stress relaxation (as rotation ceased during periods two and four). The precise step-by-step procedure used to obtain transient shear data using the RDS-II rheometer is given in Cato [6].

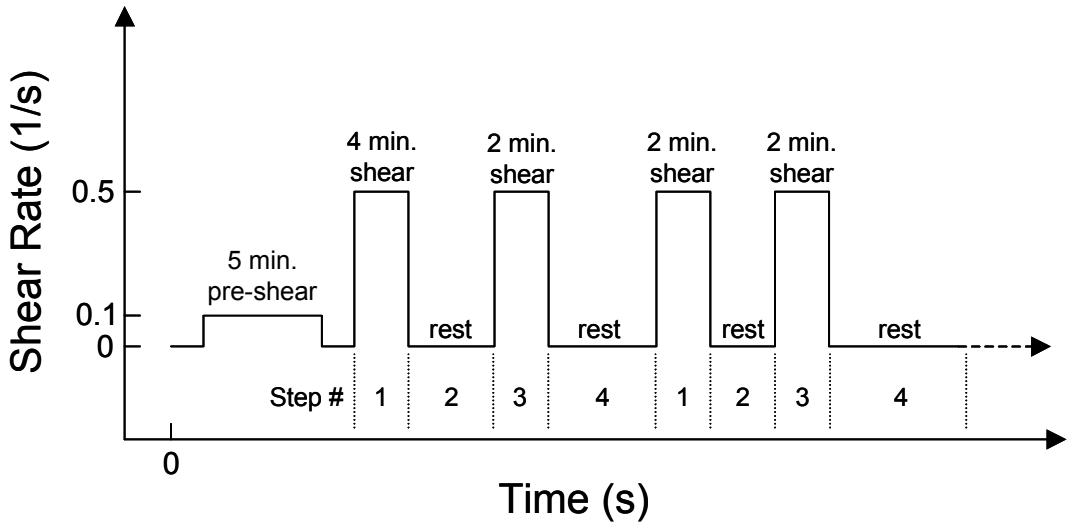

Figure 1. Typical sequence, of shear and rest periods, during transient experiments

Results and Discussion -- Experimental

The steady rheological measurements using the ARES showed that the AR mesophase is shear thinning, with a slope ranging from 0.4 - 0.5, at rates below 1 s^{-1}. However, at higher shear rates the viscosity becomes constant. As seen in Figure 2, the viscosity undergoes a distinct hesitation or “kink” within this transition. It can also be seen that the location of the transition region, and hence the kink, shifts to higher shear rates as the temperature is increased.

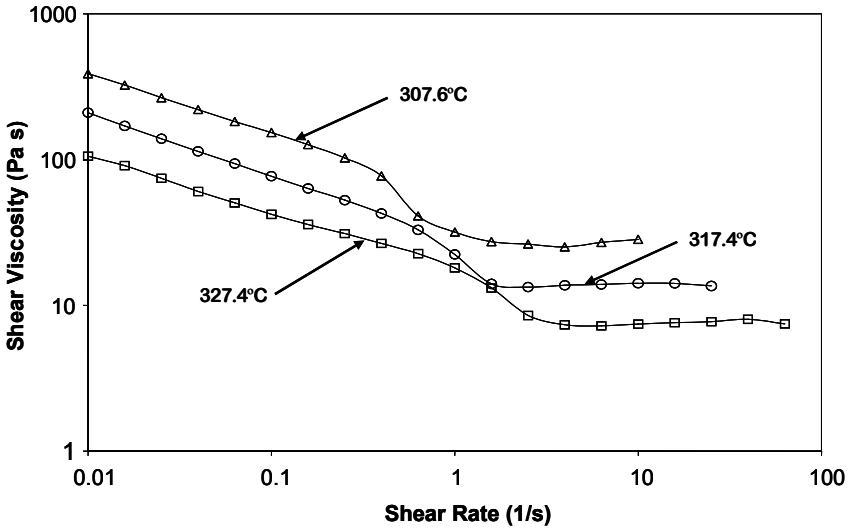

Figure 2. Steady shear viscosity of mesophase measured on the ARES rheometer

As Figure 3 shows, the measured first normal stress difference is negative at low shear rates. The shear rate region over which the first normal stress difference transitions from negative to positive corresponds to the same region in which the shear viscosity kink is observed. In a parallel study, mesophase samples were quick-frozen during typical rheological experiments at shear rates less than, approximately equal to, and greater than the kink [7]. The molecular orientation within these samples was measured using standard optical techniques. The analysis revealed an orientation change of the poly-domain structure at shear rates where the kink was observed. This orientation change results in a high viscosity to low viscosity transition. This viscosity transition would appear to be responsible for the kink phenomena [7].

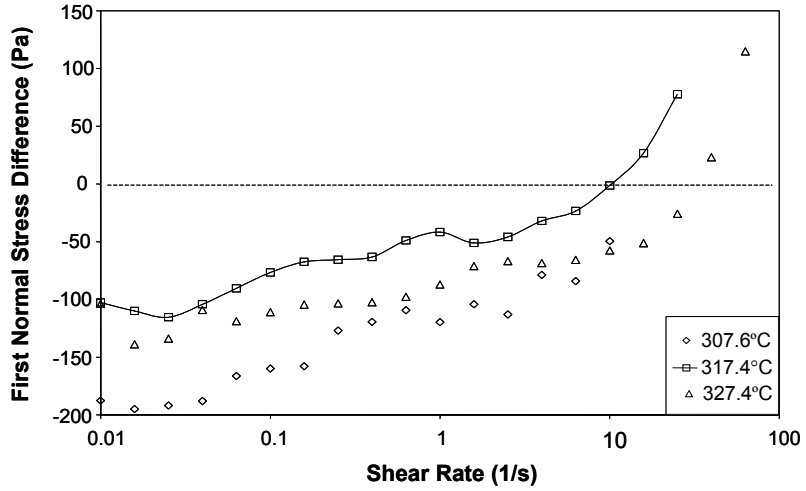

Figure 3. First normal stress difference measured on the ARES rheometer

As previously mentioned, the transient shear rheology of mesophase pitch was examined using the RDS-II rotational rheometer. A typical shear stress response for

mesophase pitch is shown in Figure 4. After the initiation of shear flow the stress response shows a peak that relaxes towards the steady state shear stress, τ_{ss}. After cessation of shear flow the stress response drops to zero over a time period of about 10-20 seconds. Studies on mesophase pitch and other liquid crystals have shown that the initial stress peak increases as the rest time increases [3],[9]. This behavior is attributed to the poly-domain structure that is disrupted during shear and then relaxes back during the rest periods ([9],[5]).

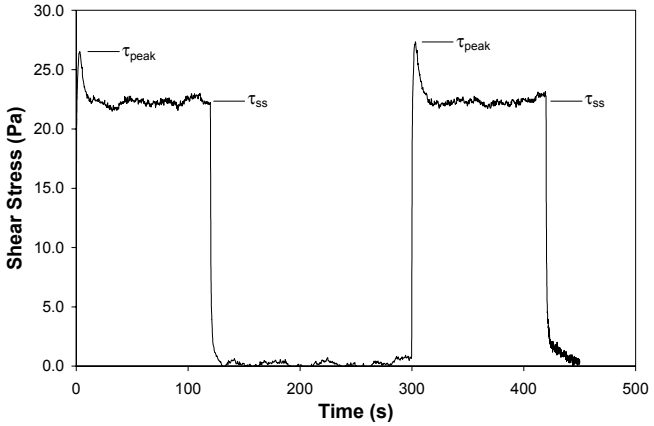

Figure 4. Transient shear stress response at 312.1°C and a shear rate of 0.5 s^{-1}

The transient stress response of LCPs during step shear is dependent upon whether the nematic fluid is of the flow tumbling or the flow aligning type. Flow tumbling can cause the director to rotate in the shear plane, oscillate in the shear plane, or become aligned in the flow. Flow aligning fluids only achieve a time independent director orientation. The transient shear response of tumbling nematics is characterized by oscillations in both the shear stress and first normal stress difference while flow aligning fluids only exhibit an overshoot before reaching a steady state [10].

As is apparent in Figure 4, oscillations in the shear stress were not present for this mesophase pitch, indicating that mesophase is flow aligning. This response was unexpected based on past modeling studies by Marrucci and Maffettone ([11], [12]) and Singh and Rey ([13], [14]) where fluids that exhibit negative first normal stresses are typically of the flow tumbling type.

Theory

A Landau-de Gennes model that takes into account short range and long range energy, and flow-induced orientations has been adapted to describe the flow behavior of flow-aligning, thermotropic, discotic, nematic, liquid crystals as models of carbonaceous mesophases [15]. The dynamics of the tensor order parameter is given by the following sum of flow **F**, short range $\mathbf{H}^{sr}$, and long range $\mathbf{H}^{lr}$ contributions [15]:

$$\hat{\mathbf{Q}} = \mathbf{F}(\mathbf{Q}, \nabla\mathbf{v}) + \mathbf{H}; \quad \mathbf{H} = \mathbf{H}^{sr}\left(\mathbf{Q}, \overline{\mathrm{D}}_r(\mathbf{Q})\right) + \mathbf{H}^{lr}(\nabla\mathbf{Q}) \tag{1}$$

(i) flow contribution **F**:

$$\mathbf{F}(\mathbf{Q},\nabla\mathbf{v}) = \tfrac{2}{3}\beta\mathbf{A} + \beta\left[\mathbf{A}\cdot\mathbf{Q} + \mathbf{Q}\cdot\mathbf{A} - \tfrac{2}{3}(\mathbf{A}:\mathbf{Q})\mathbf{I}\right] - \tfrac{1}{2}\beta\left[(\mathbf{A}:\mathbf{Q})\mathbf{Q} + \mathbf{A}\cdot\mathbf{Q}\cdot\mathbf{Q} + \mathbf{Q}\cdot\mathbf{A}\cdot\mathbf{Q} + \mathbf{Q}\cdot\mathbf{Q}\cdot\mathbf{A} - \{(\mathbf{Q}\cdot\mathbf{Q}):\mathbf{A}\}\mathbf{I}\right] \quad (2)$$

(ii) short-range elastic contribution $\mathbf{H}^{sr}$:

$$\mathbf{H}^{sr}\left(\mathbf{Q},\overline{D}_r(\mathbf{Q})\right) = -6\overline{D}_r\left[(1-\tfrac{1}{3}U)\mathbf{Q} - U\mathbf{Q}\cdot\mathbf{Q} + U\{(\mathbf{Q}:\mathbf{Q})\mathbf{Q} + \tfrac{1}{3}(\mathbf{Q}:\mathbf{Q})\mathbf{I}\}\right] \quad (3)$$

(iii) long-range elastic contribution $\mathbf{H}^{lr}$:

$$\mathbf{H}^{lr}(\mathbf{Q}) = 6\overline{D}_r\left[\frac{L_1}{2ckT}\nabla^2\mathbf{Q} + \frac{1}{2}\frac{L_2}{c\kappa T}\left[\nabla(\nabla\cdot\mathbf{Q}) + \{\nabla(\nabla\cdot\mathbf{Q})\}^T - \tfrac{2}{3}\mathrm{tr}\{\nabla(\nabla\cdot\mathbf{Q})\}\mathbf{I}\right]\right] \quad (4)$$

$$\overline{D}_r = \frac{Dr}{\left(1-\frac{3}{2}\mathbf{Q}:\mathbf{Q}\right)} \quad (5)$$

Here **A**, L_i (i=1,2), U and β are the rate of deformation tensor, the Landau coefficients, the nematic potential and the molecular shape parameter, respectively. The dimensionless numbers Er (Ericksen number) and energy ratio R [16]:

$$Er = \frac{\dot{\gamma}H^2 ckT^*}{2L_1 D_r} \qquad R = \frac{3H^2 ckT^*}{L_1} \quad (6a,b)$$

give the ratio of viscous flow effects to long-range order elasticity, and short-range order elasticity to long-range order elasticity, respectively (H is the characteristic distance between the two plates (see figure 5) , V is the constant velocity of the top plate and T^* is the isotropic-nematic transition temperature).

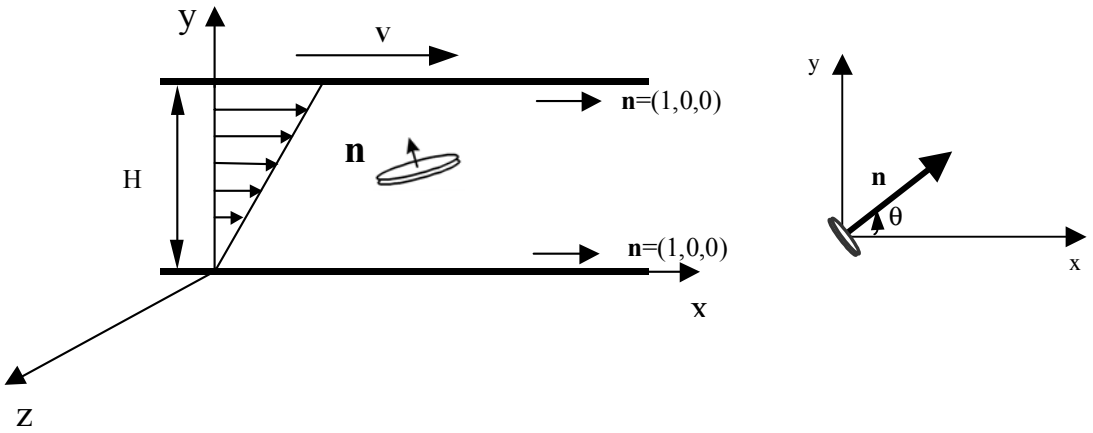

Figure 5. Definition of the flow geometry and coordinates system for simple shear flow.

A unified expression for the extra stress tensor is used. The total extra stress tensor $\mathbf{t}^t$ for liquid crystalline materials is given by the sum of symmetric viscoelastic stress tensor $\mathbf{t}^s$, anti-symmetric stress tensor, and Ericksen stress tensor $\mathbf{t}^{Er}$:

$$\mathbf{t}^t = \mathbf{t}^s + \mathbf{t}^a + \mathbf{t}^{Er} \quad (7)$$

The symmetric visco-elastic stress tensor $\mathbf{t}^{s}$ is expressed as a sum of a symmetric viscous stress contribution $\mathbf{t}^{v}$ and an elastic stress contribution $\mathbf{t}^{e}$ [17] as:

$$\mathbf{t}^{S} = \mathbf{t}^{V} + \mathbf{t}^{e} \tag{8}$$

The stress contribution $\mathbf{t}^{v}$ found is given by:

$$\begin{aligned}\mathbf{t}^{v} &= \nu_1\mathbf{A} + \nu_2\left\{\mathbf{Q}\cdot\mathbf{A} + \mathbf{A}\cdot\mathbf{Q} - \tfrac{2}{3}(\mathbf{Q}:\mathbf{A})\mathbf{I}\right\} + \\ &\quad \nu_4\left[(\mathbf{A}:\mathbf{Q})\mathbf{Q} + \mathbf{A}\cdot\mathbf{Q}\cdot\mathbf{Q} + \mathbf{Q}\cdot\mathbf{A}\cdot\mathbf{Q} + \mathbf{Q}\cdot\mathbf{Q}\cdot\mathbf{A} + \left\{(\mathbf{Q}\cdot\mathbf{Q}):\mathbf{A}\right\}\mathbf{I}\right]\end{aligned} \tag{9}$$

where ν_1, ν_2, ν_4 are viscosities coefficients. Characteristic values for these viscosities coefficients for discotic nematic liquid crystals can be found by mapping the total stress tensor with the stress tensor given by the Leslie-Ericksen vector theory [18]. The elastic contribution $\mathbf{t}^{e}$ that couples stress to the molecular field **H** is given as:

$$\begin{aligned}\mathbf{t}^{e} &= (ckT)\left[-\frac{2}{3}\beta\,\mathbf{H} - \beta\left\{\mathbf{H}\cdot\mathbf{Q} + \mathbf{Q}\cdot\mathbf{H} - \frac{2}{3}(\mathbf{H}:\mathbf{Q})\,\mathbf{I}\right\}\right. \\ &\left. + \frac{1}{2}\beta\left[(\mathbf{H}:\mathbf{Q})\mathbf{Q} + \mathbf{H}\cdot\mathbf{Q}\cdot\mathbf{Q} + \mathbf{Q}\cdot\mathbf{H}\cdot\mathbf{Q} + \mathbf{Q}\cdot\mathbf{Q}\cdot\mathbf{H} - \left\{(\mathbf{Q}\cdot\mathbf{Q}):\mathbf{H}\right\}\mathbf{I}\right]\right]\end{aligned} \tag{10}$$

The antisymmetric contribution $\mathbf{t}^{a}$ arises whenever **H.Q** is not symmetric, and is given as [19]:

$$\mathbf{t}^{a} = ckT(\mathbf{H}\cdot\mathbf{Q} - \mathbf{Q}\cdot\mathbf{H}) \tag{11}$$

The Ericksen stress contribution $\mathbf{t}^{Er}$ arises from the long range elasticity and is given as:

$$\mathbf{t}^{Er} = -\frac{\partial f}{\partial \nabla\mathbf{Q}} : (\nabla\mathbf{Q})^{T} = \left[-L_1\nabla\mathbf{Q} : (\nabla\mathbf{Q})^{T} - L_2(\nabla\cdot\mathbf{Q})\cdot(\nabla\cdot\mathbf{Q})^{T}\right] \tag{12}$$

The dimensionless first normal stress difference (N_1^{*}) and the dimensionless apparent shear viscosity (η^{*}) used to characterize the steady shear rheological material functions are given by:

$$N_1^{*} = t_{xx}^{*} - t_{yy}^{*} = \frac{t_{xx} - t_{yy}}{ckT^{*}} \tag{13}$$

$$\eta^{*} = \frac{t_{yx}}{\dot{\gamma}}\cdot\frac{6Dr}{ckT^{*}} \tag{14}$$

Results and Discussion -- Theory

We present numerical results for the rheological response as a function of shear rate and strain, when the director **n** anchoring at the walls is fixed along the flow direction (see figure 5). In the present work the parametric values are set at: U=4.5, β = -1.2 (flow aligning system), R=10^5 and viscosities coefficients: $\nu_1^{*}=1$, $\nu_2^{*}=-1$, $\nu_4^{*}>0$.

Figure 6 shows the dimensionless shear viscosity η^{*} as a function of the Ericksen number. The apparent shear viscosity is shear thinning at low shear rates and reaches a plateau at higher shear rates. The shear viscosity behavior at steady state is qualitatively similar to data obtained for mesophase pitches and follows the three region Onogi and Asada's model of LCs. The high Er plateau is given by the alignment

viscosity η_{al} corresponds to an orientation along the alignment angle $\theta=\theta_{al}$ (orientation angle) (for details see [18]).

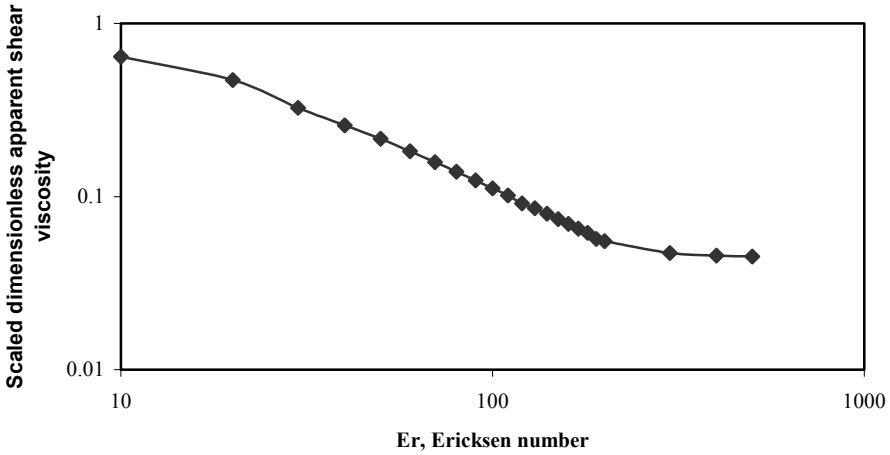

Figure 6. Predicted dimensionless apparent shear viscosity function of Ericksen number

The shear thinning corresponds to the competition between the elasticity and flow and the high shear rate plateau corresponds to the alignment regime, where the flow dominates.

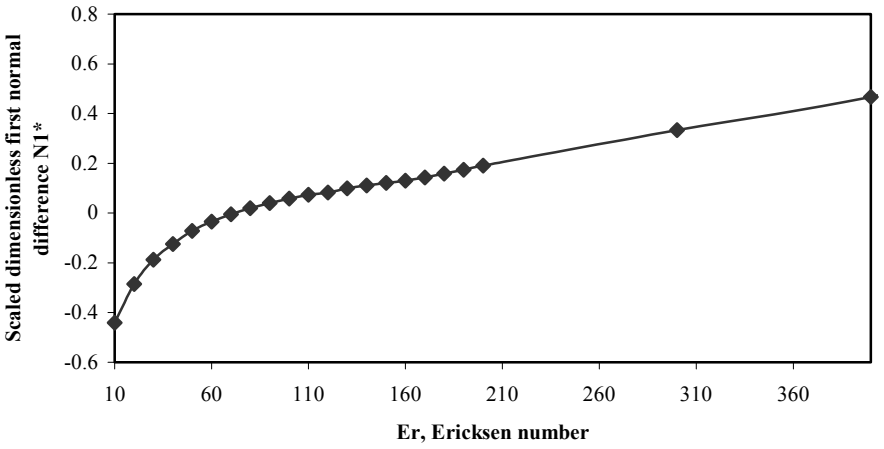

Figure 7. Predicted dimensionless first normal stress difference function of Ericksen number

Figure 7 shows the dimensionless first normal stress difference as a function of the Ericksen number. At low shear rates (Er), the values of the first normal stress

difference increase, and subsequently at Er=100 there is a sign change transition. The first normal stress difference exhibits a strong non-Newtonian behaviour, including the sign change with increasing shear rate (Er). At high shear rates, N_1 is a linear functions of the shear rate: $N_1 \propto \dot{\gamma}$, which is typical for LC and is in agreement with the experimental results. The sign change in N_1 is a direct result of nonlinearity. From equation (9) it follows that N_1 is a scalar function of **QQ** and hence normal stress sign changes can appear whenever the director components (i.e, (n_x,n_y)) change sign.

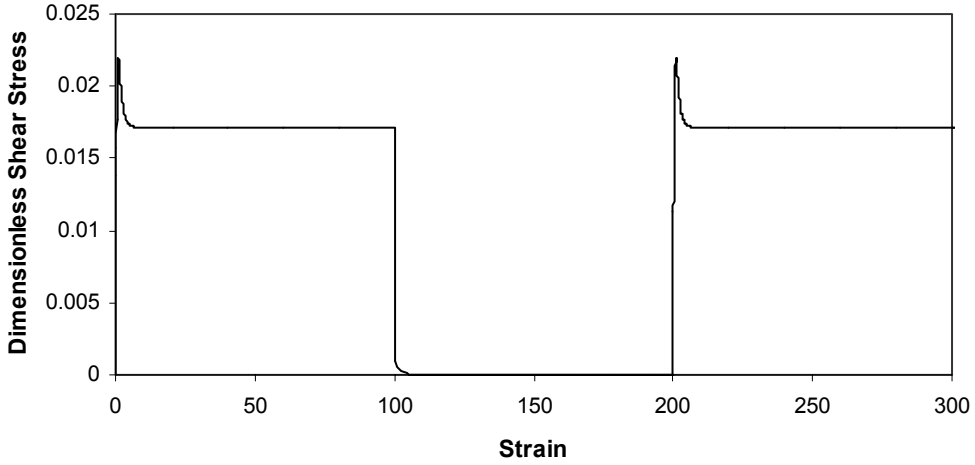

Figure 8. Predicted transient shear response in step shear flow for Er=500.

Figure 8 shows the transient evolution of the dimensionless shear stress τ_{xy} as a function of strain for Er=500, in a step shear flow. For higher Er numbers, flow dominates, the director at the midplane reaches the flow alignment angles, and an overshoot is predicted [20]. The strain ($\gamma = \dot{\gamma}\, t$) where the overshoot occurs corresponds to the orientation angle in the bulk (y*=0.5) of 45^o [20]. These results are in agreement with the transient rheology experiments.

Conclusions

The orientation-controlled steady and transient shear rheology of discotic, nematic liquid crystals that emerges under the absence of molecular order variations has been characterized. The set of rheological and structural data calculated under well controlled conditions provide the opportunity to show that the theory is capable of realistic predictions for the rheology of flow aligning liquid crystals. The predicted shear viscosity behavior at steady state is qualitatively similar to data obtained for mesophase pitches and follows Onogi and Asada's three-region model of LCs.

The predicted first normal stress difference exhibits a strong non-Newtonian behavior, including a sign change with increasing shear rate (Er). At high shear rates, N_1 follows $N_1 \propto \dot{\gamma}$, typical for LC, in agreement with the experimental results. The predicted

transient rheological response, characterized by a single overshoot and monotonic relaxation also agrees with the experimental data.

References

[1] Fathollahi B. Flow-Induced Microstructures in the Spinning of Carbonaceous Mesophase, a Discotic Nematic Liquid Crystal, Ph.D. Dissertation, University of California, San Diego (1996).

[2] Fathollahi B, and White JL. Polarized-Light Observation of Flow-Induced Microstructures in Mesophase Pitch, J. Rheol 1994;38:1591-1607.

[3] Fleurot O. High Thermal Conductivity Carbon Fibers Melt Spun from Naphthalene-Based Mesophase, M.S. Thesis, Clemson University, Clemson, SC (1993).

[4] Fleurot O. The Viscoelastic Flow Behavior of Pitches, Ph.D. Dissertation, Clemson University, Clemson, SC (1998).

[5] Fleurot O, and Edie DD. Steady and Transient Rheological Behavior of Mesophase Pitches, J. Rheol 1998;42(4): 781-793.

[6] Cato AD. Flow and Deformation Behavior of Mesophase Pitch, Ph.D. Dissertation, Clemson University, Clemson, SC (2002).

[7] Cato AD and Edie DD. Flow Behavior of Mesophase Pitch, Carbon 2003;41: 1411-1417.

[8] Grizzuti N, Cavella S, and Cicarelli P. Transient and Steady-State Rheology of a Liquid Crystalline Hydroxypropylcellulose Solution, J. Rheol. 1990;34(8):1293-1310.

[9] Viola GG and Baird DG. Studies on the Transient Shear Flow Behavior of Liquid Crystalline Polymers, J. Rheol. 1986; 30: 601-628.

[10] Ternet DJ, Larson RG, and Leal LG. Flow-aligning and Tumbling in Small-molecule Liquid Crystals: Pure Components and Mixtures, Rheol. Acta.1999; 38: 183-197.

[11] Marrucci G and Maffettone PL. Nematic Phase of Rodlike Polymers. I. Prediction of Transient Behavior at High Shear Rates, J.Rheol. 1990; 34(8): 1217-1230.

[12] Marrucci G and Maffettone PL. Nematic Phase of Rodlike Polymers. II. Polydomain Preditions in the Tumbling Regime, J.Rheol. 1990; 34(8): 1231-1244.

[13] Singh AP and Rey AD. Microstructure Constitutive Equation for Discotic Nematic Liquid Crystalline Materials, Part I: Selection Procedure and Shear Flow Predictions, Rheol. Acta. 1998; 37: 30-45.

[14] Singh AP and Rey AD. Microstructure Constitutive Equation for Discotic Nematic Liquid Crystalline Materials, Part II: Microstructure-rheology Relations, Rheol. Acta. 1998; 37: 374-386.

[15] Singh AP and Rey A.D. Effect of Long Range Elasticity and Boundary Conditions on Microstructural Response of Sheared Discotic Mesophases, J Non-Newt. Fluid Mech. 2000;94: 87-111.

[16] Tsuji T. and Rey A.D. Effect of long-range order on sheared liquid crystalline materials. Part I: Compatibility between tumbling behavior and fixed anchoring, J Non-Newt. Fluid Mech. 1997; 73:127-152.

[17] de Gennes P.G. and Prost J. The physics of Liquid Crystals, 2nd edn. Clarendon Press, Oxford, 1993.

[18] Grecov D. and Rey A.D. Computational Rheology for Discotic Nematic Liquid,Crystals Mol. Cryst.Liq. Cryst. 2002; 391(1): 57-97.
[19] Farhoudi Y. and Rey A.D. Shear flows of nematic polymers .1. orienting modes, bifurcations, and steady-state rheological predictions,J Rheol 1993;37: 289-314.
[20] Grecov D. and. Rey A.D Transient Rheology of Discotic Mesophases, Rheol. Acta 2003; 42(6): 590-604.